

Identification of a Griffiths-like phase and its evolution in the substituted pyrochlore iridates $Y_2Ir_{2-x}Cr_xO_7$ ($x = 0.0, 0.05, 0.1, 0.2$)

Vinod Kumar Dwivedi *

*Materials Science Programme, Indian Institute of Technology Kanpur, Kanpur 208016, India;
and Department of Physics, Indian Institute of Science, Bengaluru 560012, India*

 (Received 17 December 2022; revised 9 February 2023; accepted 5 April 2023; published 12 April 2023)

We report the Griffiths phase (GP)-like state along with a cluster-glass-like state in geometrically frustrated antiferromagnetic Cr-substituted $Y_2Ir_2O_7$ pyrochlore iridates. The strength of the GP-like behavior increases with substitution. Interestingly, isothermal remanent magnetization suggests the Ising-like interaction of spins in the GP region. The GP-like state is not attributed to the structural disorder as substitution of Cr does not induce any structural change. Then the spin coupling between $Cr^{3+} \leftrightarrow Cr^{3+}$, $Ir^{4+} \leftrightarrow Ir^{4+}$, $Ir^{4+} \leftrightarrow Cr^{3+}$, and $Ir^{4+} \leftrightarrow Ir^{5+}$ leads to the competition between antiferromagnetic and ferromagnetic correlations. It gives rise to Ruderman-Kittel-Kasuya-Yosida (RKKY)-like interaction between Cr^{3+} local magnetic moments mediated by itinerant Ir conduction electrons, hence, as a result, GP and cluster-glass-like states emerge.

DOI: [10.1103/PhysRevB.107.134413](https://doi.org/10.1103/PhysRevB.107.134413)

I. INTRODUCTION

A spin glass (SG) is known as a randomly distributed mixed interacting bond [antiferromagnetic (AFM) and ferromagnetic (FM)] characterized by a collective freezing of the spins at a definite temperature T_{SG} below which a highly irreversible metastable frozen state appears without the usual magnetic long-range ordering, where each and every spin resides in a frustrated state [1]. SGs show a phase transition from a high-temperature paramagnetic (PM) state into a low-temperature glassy state with exponential relaxation of spins. Long ago, it was reported that a low-temperature magnetic state fuses into a state whose correlation functions follow nonexponential tails [2] due to the emergence of the same unfrustrated clusters favoring the growth of the Griffiths phase (GP) [3,4] in the magnetization, sandwiched between the SG and PM state.

The GP was initially suggested for randomly diluted Ising ferromagnets, where only a tiny part of the lattice sites are filled with spins and remaining fractions are either empty or occupied with nonmagnetic ions. Further, it has been shown that disorder suppresses the magnetic transition from its clean value of T^* (Griffiths temperature) to long-range magnetic ordering temperature T_C [3]. GP is characterized by the formation of magnetically ordered rare regions within the global PM matrix at $T_C < T < T^*$. Such a system contains a sharp downturn at the high-temperature regime in inverse magnetic susceptibility $1/\chi$ versus T curve below T^* [5]. The physics of the GP is closely related to quenched disorder and competing interactions [5–11]. In fact, GP behavior has mostly been reported in diluted FM systems with a positive value of Curie-Weiss (CW) temperature θ_{CW} , however, there are *very limited* experimental reports on GP exhibiting negative values

of CW temperature θ_{CW} in antiferromagnetic (AFM) systems [11–15].

In pyrochlore iridates $R_2Ir_2O_7$ ($R = Y, Bi$, rare-earth elements), the interplay of spin-orbit coupling, electronic correlation, and crystal electric field comparable at energy scales offer many emergent quantum phases [16–20], and can be achieved by tuning the strength of relative energy scales via chemical substitution [21–30], reducing the particle sizes [31–35], lattice mismatch induced strain effects [9,36], etc. Although, theoretically $Y_2Ir_2O_7$ (YIO) is expected to be a candidate of magnetic Weyl semimetal [17] with an all-in/all-out AFM ground state. Moreover, neutron diffraction and inelastic scattering measurements of a YIO powder sample [37,38] do not show any sign of long-range magnetic ordering for small moments of $Ir^{4+}(5d^5)$ within the measurement limit of instrument. However, these measurements do not rule out long-range magnetic order, but do put an upper limit for the Ir^{4+} ordered moment of $\sim 0.2 \mu_B/Ir$ (for a magnetic structure with wave vector $Q \neq 0$) or $\sim 0.5 \mu_B/Ir$ (for $Q = 0$) based on the structural refinements of neutron powder diffraction pattern. On the other hand, muon spin relaxation (μSR) is very sensitive to probe internal magnetic fields as a result of ordered magnetic moments or random fields that are static or fluctuating (of a few Gauss) with time due to its large gyromagnetic ratio. The zero-field μSR measurements of the YIO powder sample shows the appearance of spontaneous muon spin precessions below transition temperature, confirming the long-range magnetic ordering [38–41]. Recently, the glass-like state [42] in YIO has also been reported, where the chemical doping of a magnetic $Ru^{4+}(4d^4)$ ion [23], a nonmagnetic $Ti^{4+}(3d^0)$ ion [23] at the magnetic $Ir^{4+}(5d^5)$ site, and the substitution of magnetic $Pr^{3+}(4f^2)$ for the nonmagnetic $Y^{3+}(4d^0)$ -site [24] separately enhances the magnetic relaxation rate. Moreover, it has also been shown that YIO exhibits a weak FM component along with a large AFM ground state [19–21,29,30,43]. Despite these advances, a conclusive

*vinodd.iitbombay@gmail.com

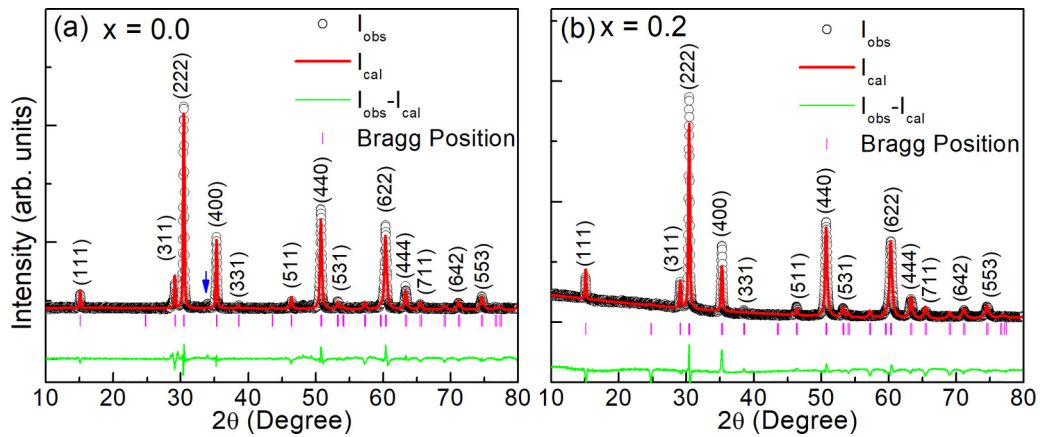


FIG. 1. Room temperature XRD pattern of (a) $x = 0.0$, and (b) $x = 0.2$ samples. Arrow represents Y_2O_3 parasitic phase.

understanding of the precise nature of the magnetic state is not yet fully established.

In this paper, we attempt to bridge the lacking by our latest finding of gradual substitution of magnetic ion Cr^{3+} ($3d^3$) at the Ir^{4+} ($5d^5$) magnetic site in geometrically frustrated AFM pyrochlore iridates YIO, i.e., $Y_2Ir_{2-x}Cr_xO_7$ (YICO). We find that YIO shows GP along with the cluster-glass-like state and these properties enhance on increasing with doping concentration. This substitution would produce the following effects: (1) it would bring magnetic impurity in the Ir^{4+} sublattice, (2) it would alter the concentration of the charge carrier which, in turn, changes the $3d - 5d$ magnetic exchange interaction between the local Cr^{3+} moments (randomly distributed in the Ir sublattice) and itinerant Ir^{4+} conduction electrons, and (3) since Cr^{3+} ($3d^3$) have relatively larger strengths of electronic correlation and low values of spin-orbit coupling compared to Ir^{4+} ($5d^5$), the substitution will likely induce disorder. Our results show the presence of magnetically ordered rare regions at $T_C < T < T^*$, supporting the formation of a GP-like state

in the YIO sample. The strength of magnetically ordered rare regions enhances as doping concentration of Cr increases. Interestingly, the nature of interacting spins in the GP regime is found to be Ising-like. In addition, the cluster-glass-like state at low temperature is also observed.

II. EXPERIMENTAL METHOD

Polycrystalline samples of the YICO series ($x = 0.0, 0.05, 0.1, 0.2$) were synthesized using the conventional solid state reaction route following the protocols described elsewhere [27,44]. A high-purity stoichiometric amount of starting materials Y_2O_3 , IrO_2 , and Cr_2O_3 were mixed, ground, pelletized, and heated in air at $1000^\circ C$ for 100 h, at $1050^\circ C$ for 200 h with several intermediate grinding with heating and cooling rate $3^\circ C/min$. Room-temperature powder x-ray diffraction (XRD) patterns were measured to check the structural phase formation of the samples using a PANalytical XPertPRO diffractometer with $Cu - K_\alpha$ radiation ($\lambda = 1.54056 \text{ \AA}$).

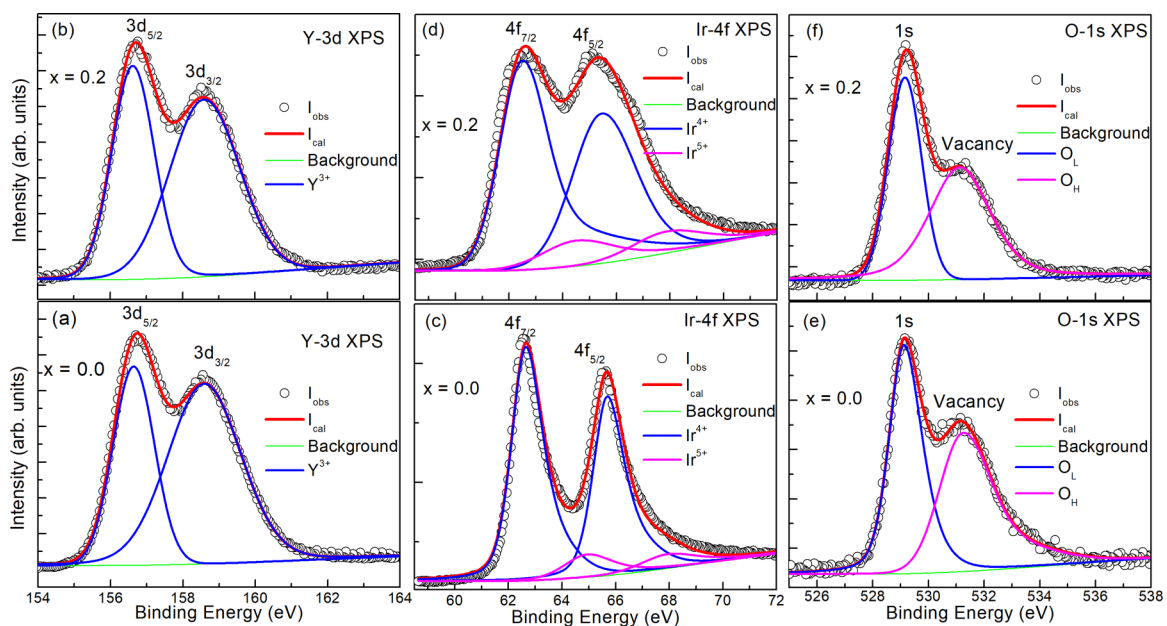


FIG. 2. Deconvoluted XPS spectra measured at room temperature of (a) Y-3d, (b) Ir-4f, and (c) O-1s of two representative samples $x = 0.0$ and 0.2 of the series YICO.

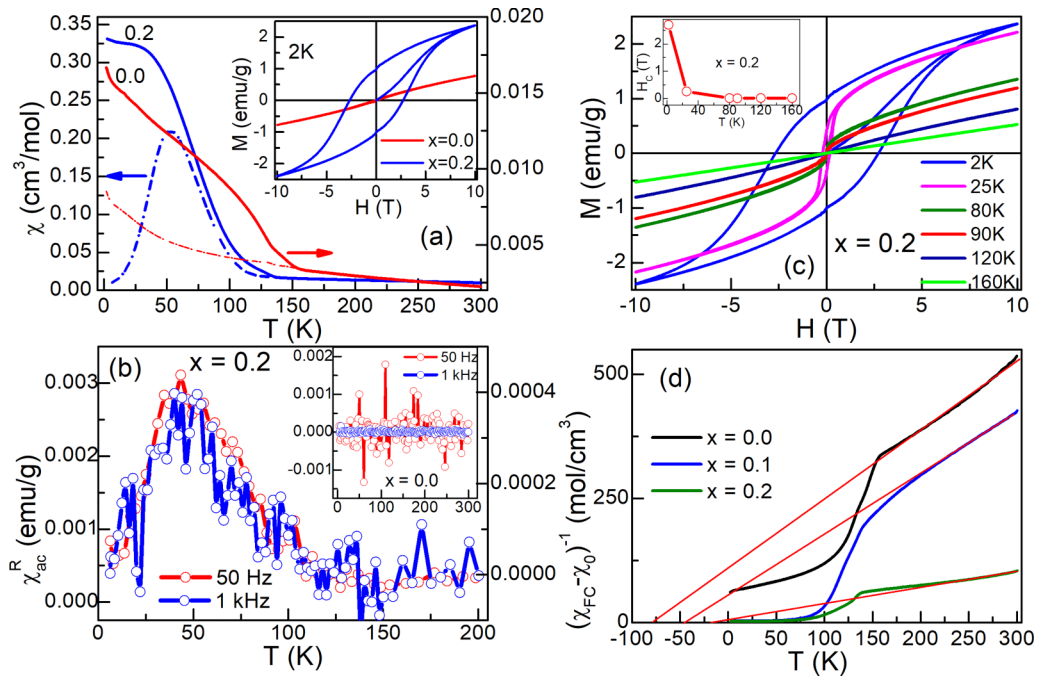


FIG. 3. (a) Variation of magnetic susceptibility ($\chi = M/H$) with temperature measured in the presence of $H = 1$ kOe following the zero-field-cooled (ZFC) and field-cooled (FC) protocol shown by short dash dot line and solid continuous line, respectively; inset shows magnetization as a function of magnetic field. (b) Real part of the ac susceptibility as a function of temperature measured at 50 Hz (right y axis) and 1 kHz (left y axis) for $x = 0.2$ sample; for $x = 0.0$, shown in inset. (c) Magnetic hysteresis loops of $x = 0.2$ sample measured at various temperatures; inset represents temperature-dependent coercive field (H_C), (d) $(\chi_{FC} - \chi_0)^{-1}$ as a function of temperature; red solid continuous lines are a guide to the eyes.

The x-ray photoelectron spectroscopy (XPS) measurements were recorded using a PHI 5000 Versa Probe II system with an energy resolution of 0.02 eV and step size 0.05 eV. dc magnetic measurements were performed between 2-350 K with a 14 T Quantum Design Physical Property Measurement System using vibrating sample magnetometry mode. The ac susceptibility measurement was carried out in a cryogenic S700X model Superconducting Quantum Interference Device magnetometer down to 5 K at frequencies 50 Hz and 1 kHz with an excitation field $H_{ac} = 0.1$ Oe and dc drive field $H_{dc} = 1000$ Oe.

III. RESULTS AND DISCUSSION

The powder XRD patterns measured at room temperature of two representative samples $x = 0.0$ and 0.2 of YICO series are shown in Figs. 1(a) and 1(b). The XRD pattern was analyzed by Rietveld refinement using the software FULLPROF, confirming the phase purity of the samples. Refinement shows a pyrochlore cubic crystal structure with $Fd\bar{3}m$ space group. For the $x = 0.0$ sample, a small impurity phase of Y_2O_3 was detected in the sample shown by the arrow in Fig. 1(a), which are in agreement with earlier literature [21,43]. For the $x = 0.2$ sample, impurity phase was not found. Y_2O_3 is diamagnetic in nature, hence it would not affect magnetic properties of the YICO series. The lattice parameter a , Ir - O - Ir bond angle obtained from refinement for $x = 0.0$ and 0.2 samples are 10.16 Å, 120°, and 10.00 Å, 108°, respectively. It suggests reduction of the lattice constant and bond angle with substitution of Cr. Figures 2(a)–2(f) display the XPS spectra

of $x = 0.0$ and 0.2 samples. The Y-3d XPS peaks shown in Figs. 2(a) and 2(b) show a single feature suggesting the presence of Y^{3+} in both samples, which is in agreement with earlier reports [26–28]. Figures 2(c) and 2(d) show deconvoluted Ir-4f XPS spectra which can be fitted with two sets of doublets related to the contribution from Ir^{4+} and Ir^{5+} , which is in agreement with reports [26–28,31,32]. We find that for the $x = 0.2$ sample, the contribution from Ir^{5+} is increased, indicating the copresence of mixed oxidation states, i.e., Ir^{4+} and Ir^{5+} . Further support of mixed valence states can also be seen in O-1s XPS spectra [Figs. 2(e)–2(f)]. The peaks centered at binding energies 529 eV and 531.1 eV are associated as lower O_L and higher O_H binding energy peaks, respectively [22,28,32]. The O-1s XPS spectra can be fitted with a set of doublets. We observed that the ratio of O_H and O_L is enhanced in the $x = 0.2$ sample, supporting the presence of mixed oxidation states of metal ion.

Temperature-dependent magnetic susceptibility of two representative samples $x = 0.0$ and $x = 0.2$ of the YICO series is shown in Fig. 3(a). For the $x = 0.2$ sample, the ZFC magnetic susceptibility χ_{ZFC} increases gradually to a maximum around a peak temperature T_f and then decreases monotonically as temperature reduces. A clear bifurcation between χ_{FC} and χ_{ZFC} curves at an irreversibility temperature T_{irr} is observed. The cusp in χ_{ZFC} versus T curve is more prominent for $x = 0.2$ compound (~ 50 K) as compared to $x = 0.0$ (~ 130 K, hardly visible in $\chi_{ZFC} - T$ curve [27]). The value of T_{irr} and T_f is given in Table I. A sharp rise in χ_{FC} and χ_{ZFC} curves below T_{irr} for both samples suggest formation of FM clusters. Further, the magnetic transition temperature can be calculated

TABLE I. Parameters obtained from the magnetization data. FM transition temperature T_C is estimated from the minima in first derivative of χ_{FC} versus T curve. H_C estimated from $M(H)$ curve.

Sample	$x = 0.0$	$x = 0.05$	$x = 0.1$	$x = 0.2$
T^* (K)	230	240	240	245
T_{irr} (K)	160	155	145	140
T_C (K)	130	65	67	70
T_f (K)	130	46	48	50
$-\theta_{CW}$ (K)	75	70	40	10
μ_{eff}^{exp} ($\mu_B/f.u.$)	2.27	2.62	2.95	4.92
μ_{eff}^{theo} ($\mu_B/f.u.$)	1.73	2.57	2.68	2.9
H_C (T)	0.037	1.66	2.74	2.78
$GP_{norm} = \frac{T^* - T_C}{T_C}$	0.77	2.88	3.50	3.85

following the protocol given elsewhere [27], where the minimum in $d\chi_{FC}/dT$ versus T curves are attributed to the FM transition temperature T_C , while the maximum indicates AFM transition temperature T_N . The estimated values of T_C are given in Table I. Figure 3(b) shows the real component of ac susceptibility as a function of temperature of sample $x = 0.2$,

suggesting a well-defined cusp at temperature ~ 50 K similar to freezing temperature T_f of χ_{ZFC} versus T curve. However, the quality of data is not good enough to fix any frequency dependence characterizing conventional SG-like features. The ac susceptibility of the $x = 0.0$ sample is shown in the inset of Fig. 3(b) but the signal was very weak. Figure 3(c) shows the M versus H curves measured at several temperatures of the $x = 0.2$ sample. The estimated value of H_C decreases monotonously as temperature increase [inset of Fig. 3(c)] and disappear above $T_C \sim 70$ K, however, it shows huge enhancement of H_C in the glassy state. It suggests the evolution of the glassy behavior arises likely due to randomly arranged Cr ions in the Ir sublattice. Eventually, it is interesting to see that T_{irr} is far away from the T_f , and hysteresis in M versus H curves suggest formation of a cluster-glass-like behavior [45], possibly due to the coexistence of mixed oxidation states of Ir. As a result, the FM-PM transition arises due to FM super- and double-exchange interactions via $Ir^{4+}-O^{2-}-Cr^{3+}$ or $Ir^{4+}-O^{2-}-Ir^{5+}$ path, respectively, and glassy state at T_f because of $Ir^{4+}-O^{2-}-Ir^{4+}$ and $Cr^{3+}-O^{2-}-Cr^{3+}$ AFM couplings.

Further, the susceptibility of YICO series was analyzed using the modified CW law, $\chi = \chi_0 + \frac{C}{T - \theta_{CW}}$; where C , θ_{CW} , and χ_0 are the Curie constant, CW temperature,

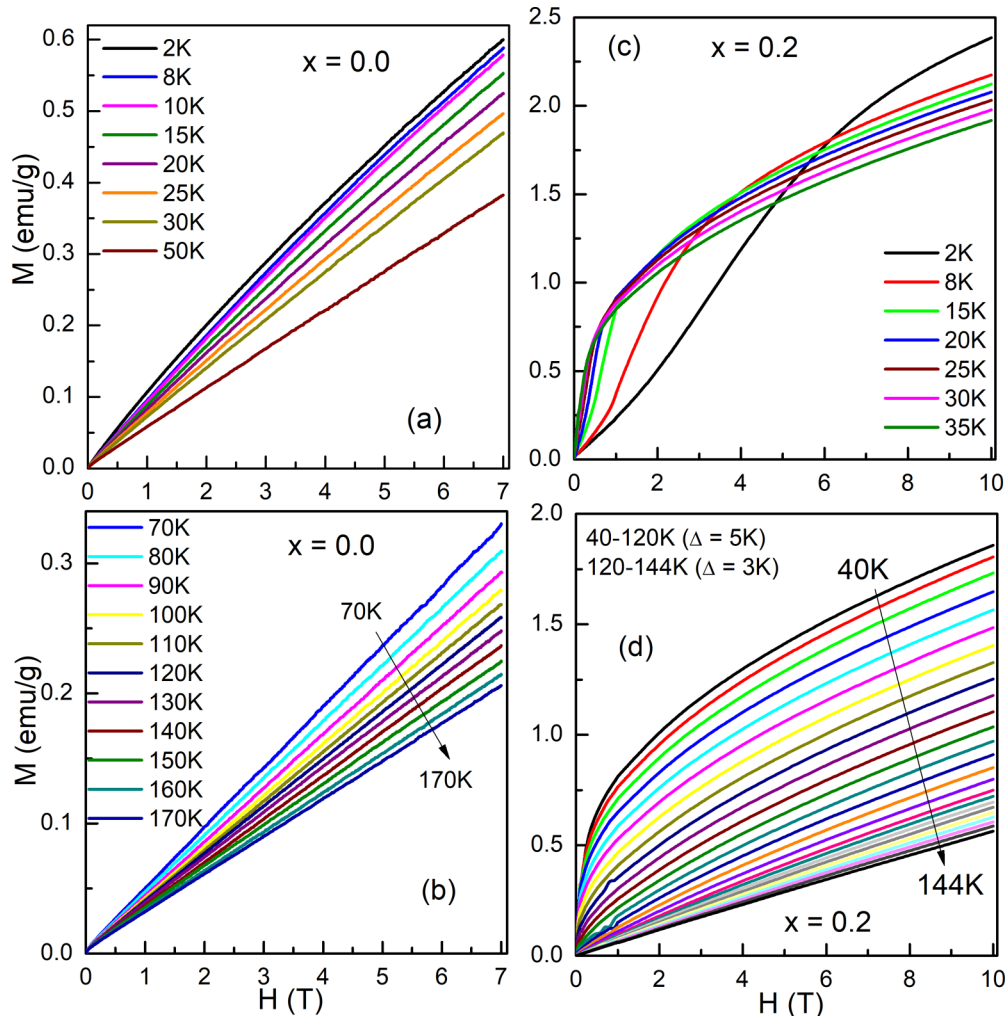


FIG. 4. Magnetic field dependence of virgin magnetization isotherms of $x = 0.0$ (a), (b) and $x = 0.2$ (c), (d) samples.

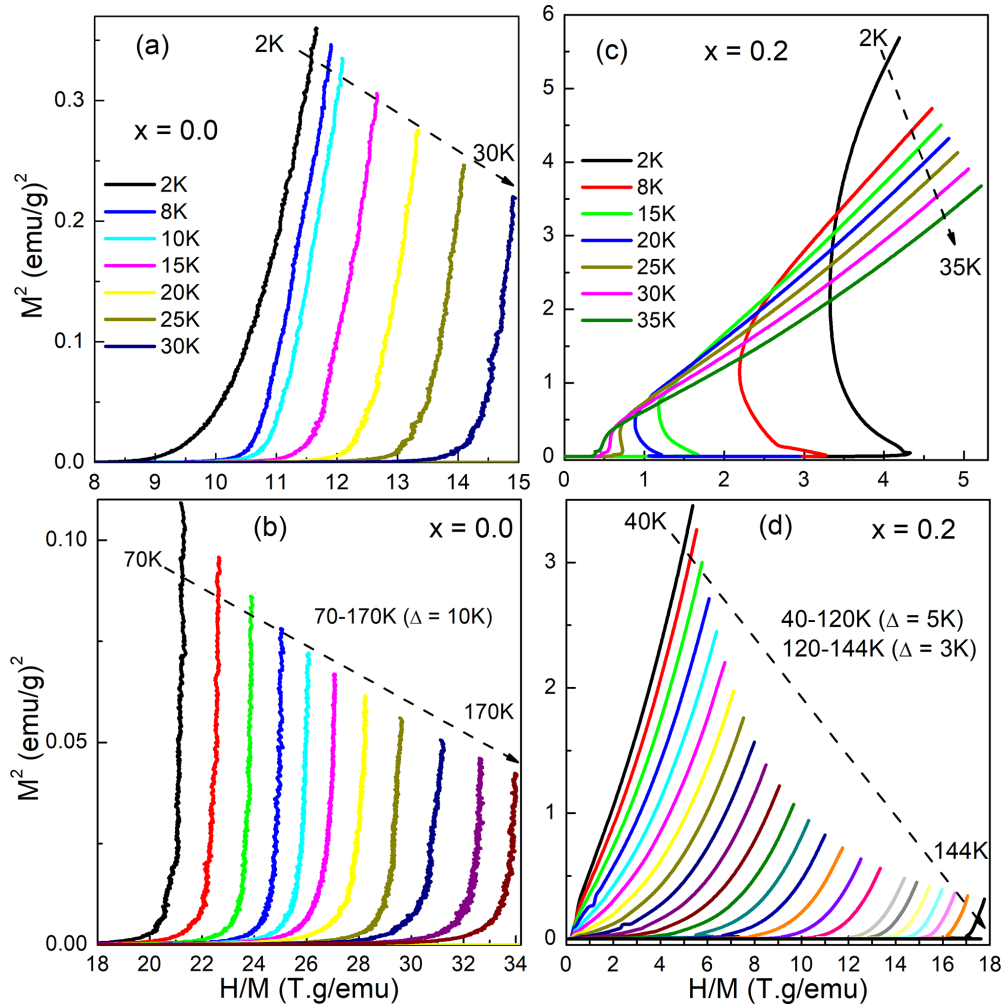


FIG. 5. Standard Arrott plots of two representative samples $x = 0.0$ (a), (b) and $x = 0.2$ (c), (d) of YICO series.

and temperature-independent susceptibility, respectively. A fit using the CW law well above T^* shown in Fig. 3(d) gives the best fitted values of important parameters are listed in Table I. The negative value of θ_{CW} for all the samples indicates AFM correlations. The observations from a closer inspection of Fig. 3(d) are: (1) Nonlinearity in the $(\chi_{FC} - \chi_0)^{-1}$ versus T curve at $T_{irr} < T < T^*$, likely due to the presence of strong crystal field. (2) $(\chi_{FC} - \chi_0)^{-1}$ versus T follows the CW law above T^* . (3) Larger values of experimental effective magnetic moments μ_{eff}^{exp} ($= \sqrt{8C} \mu_B$) than theoretical μ_{eff}^{theo} . It suggests the formation of FM clusters in the PM matrix [9]. Here the theoretical effective magnetic moment can be calculated using formulas reported elsewhere [26,29,30], i.e., $\mu_{eff}^{theo} = \sqrt{(2-x)\mu_{Ir}^2 + x\mu_{Cr}^2}$, where μ_{Ir} and μ_{Cr} are the spin-only contributed values of effective magnetic moments of Ir and Cr ions, respectively. (4) A sharp downward deviation well below T^* . (5) Marginal upward deviation in $(\chi - \chi_0)^{-1}$ versus T curves from the ideal CW behavior near T^* just before the start of downturn with lowering of temperature, similar to other systems [8,46,47]. These observations suggest GP-like behavior, i.e., formation of magnetically ordered rare regions in the global PM matrix at $T_C < T < T^*$.

Further, isothermal M versus H measurements at distinct temperatures have been carried out. All M versus H data were

recorded in ZFC condition and, before each successive magnetic isotherms, the sample was heated above T^* to eliminate the magnetic history. This protocol is *important* for pyrochlore iridates to measure the M versus H isothermal magnetization. Figures 4(a)–4(d) show the virgin isotherm magnetization curves for $x = 0.0$ (up to 7 T) and $x = 0.2$ (up to 10 T) samples at closely spaced temperatures. M versus H curves show monotonic enhancement with field without any sign of saturation for both the samples. The absolute values of M at 7 T and 2 K are estimated to be 0.6 emu/g ($0.07 \mu_B$) and 2.4 emu/g ($0.23 \mu_B$) for $x = 0.0$ and 0.2 samples, respectively. For sample $x = 0.0$, close inspection indicate a slight convex-like behavior at low temperature [Fig. 4(a)], while linear nature [Fig. 4(b)] at high temperatures. On the other hand, sample $x = 0.2$ shows a crossover at low field up to 35 K [Fig. 4(c)]. Surprisingly, we do not find linear behavior in the M versus H curve up to 170 K [Fig. 4(d)], suggesting the presence of nonparamagnetic regime.

Further, to examine the strength and nature of the complex magnetic interactions, the conventional Arrott plots [28] (M^2 versus H/M) are shown in Figs. 5(a)–5(d). A negative intercept is observed for both samples $x = 0.0$ and 0.2, suggesting the absence of spontaneous magnetization. This information is important because long-range type AFM correlations possibly

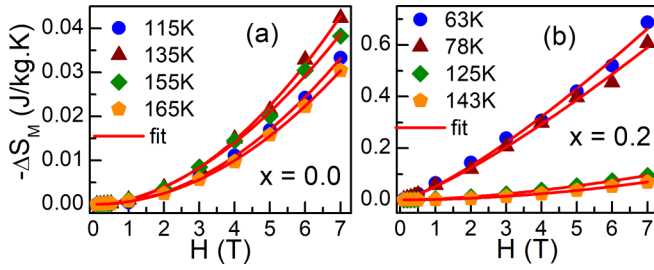


FIG. 6. $-\Delta S_M$ versus H at different temperatures of (a) $x = 0.0$ and (b) $x = 0.2$ samples; red solid line represents H^n dependence.

exhibit weak FM clusters. For the $x = 0.2$ sample, the strength of the negative intercept on the M^2 axis decreases as compared to $x = 0.0$ with lowering the temperature, suggesting the possibility of an enhanced FM signal. Interestingly, the Arrott plot shows a distorted S-like shape with negative curvature at low field (below 1 T) shown in Fig. 5(c), suggesting the complex nature of field-induced metamagnetic transition. In addition, nonstraight M^2 curves with a positive slope at low field and vertically at high field suggests the existence of short-range correlations in the proximity of AFM background in both samples.

To find further support for the GP behavior, i.e., the presence of magnetic clusters in the global PM matrix range $T_C < T < T^*$, the variation in magnetocaloric entropy change $\Delta S_M = \int_0^H (\partial M / \partial T) dH$ is estimated from M versus H isotherms. It has already been shown by the same author [27] that ΔS_M versus T measured at several fields exhibit the coexistence of conventional and inverse magnetocaloric effect in Cr-substituted YIO samples, emerging due to the coexistence and competition between the FM and AFM clusters. It is further analyzed using the prediction of mean-field theory, which suggests that ΔS_M versus H should follow the power-law [48] behavior $\Delta S_M \propto H^n$, where n is the local exponent of the entropy change. Here, for an ideal FM system, $n = 0.67$ near T_C , $n \sim 1$ well below T_C and $n = 2$ in the PM regime above T_C . We have fitted $-\Delta S_M$ versus H data using the power law shown by the red line in Figs. 6(a) and 6(b). Above T_C , the estimated values of n turn out to be (1) for the sample $x = 0.0$, 1.92 (135 K), 1.95 (155 K), and 1.98 (165 K) and (2) for sample $x = 0.2$, 1.25 (77 K), 1.65 (125 K), and 1.85 (143 K). It is obvious that the estimated value of n is less than 2 above T_C for both the samples, deviating from the ideal value of $n = 2$ for the PM regime. It suggests the presence of magnetic clusters above T_C in the global PM regime in YICO series. Here, lower values of n for the $x = 0.2$ sample indicates the presence of higher contribution of magnetic clusters in substituted samples as compared to $x = 0.0$.

To elaborate the nature of probable GP, $\frac{1}{\chi}$ versus T graph were plotted at different fields. Figures 7(a) and 7(b) show a pronounced field-dependent sharp and sudden downward deviation on approaching the magnetic transition from the high temperature PM region. The sharpness of the downturn decreases with field and is suppressed at higher field; although suppression of downturn with field is not systematic for the $x = 0.0$ sample. Such behavior is consistent with the characteristics of GP. Generally, magnetic systems exhibiting GP show: (1) Sharp downward deviation of $\frac{1}{\chi}$

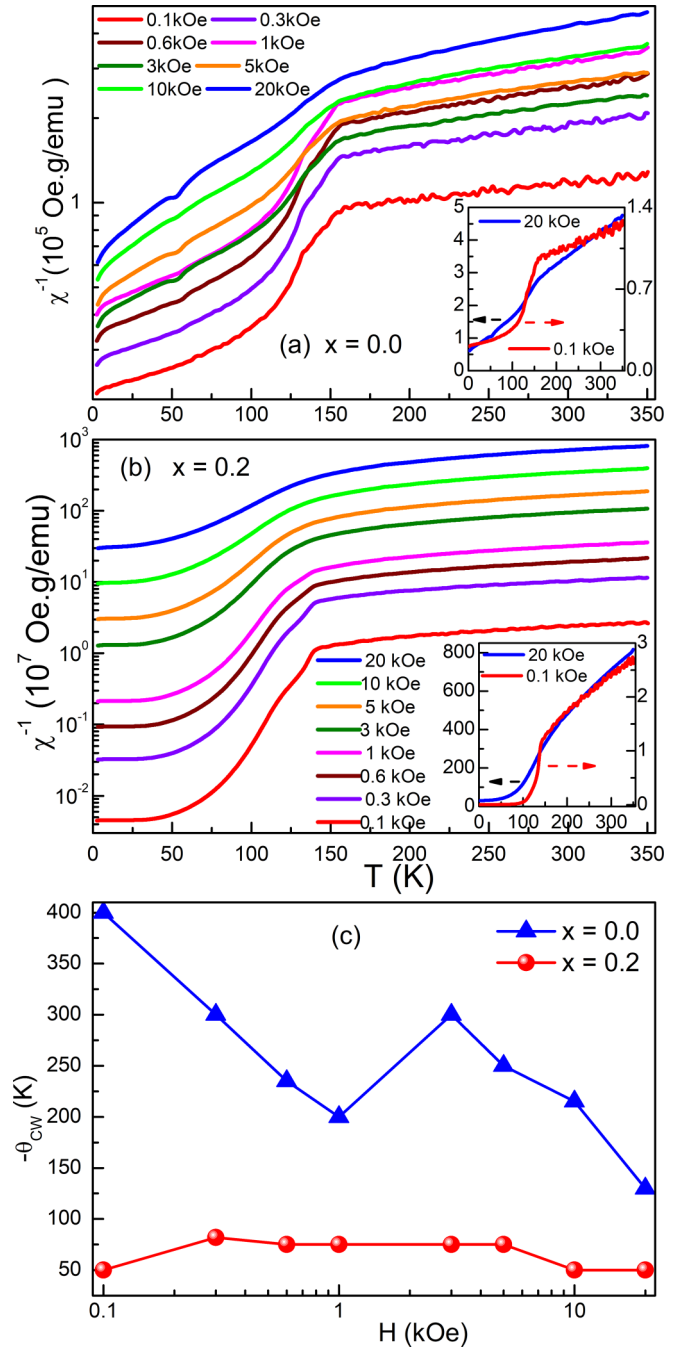


FIG. 7. Semilog plot of χ^{-1} versus T for samples (a) $x = 0.0$, (b) $x = 0.2$. Insets show same at lowest and highest fields on linear scale. (c) Variation of $-\theta_{CW}$ with field.

versus T curves from conventional CW behavior below T^* , where the sharpness of this downturn decreases as H increases, and (2) overlapping of all the $\frac{1}{\chi}$ versus T curves measured at all fields in the global PM regime above T^* . It is obvious that $\frac{1}{\chi}$ versus T curves measured at all applied magnetic fields do not overlap in the global PM regime above T^* . This only means that the effect of external magnetic field is beyond the simple mean-field behavior. The variation of $-\theta_{CW}$ with H for both samples is plotted in the Fig. 7(c), indicating that the $-\theta_{CW}$ changes with field for

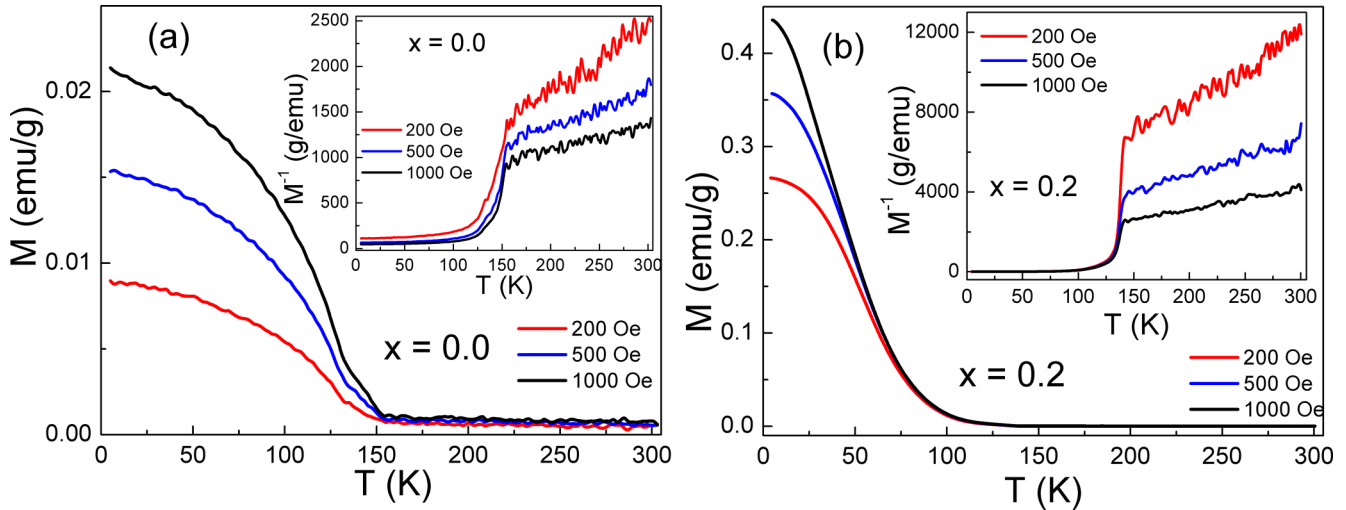


FIG. 8. Thermoremanent magnetization (TRM) as a function of temperature for (a) $x = 0.0$, and (b) $x = 0.2$ specimens; inset shows sharp downturn below T^* .

the same sample. Moreover, it could be clusters or FM impurities, but also any other interaction that might be comparable with Zeeman energy at the given field. Thus, the GP-like state appear to be an inherent characteristic of YICO.

Figures 8(a) and 8(b) show the thermoremanent magnetization of $x = 0.0, 0.2$ samples measured at different fields. The sample was cooled down to low temperature in the presence of applied field. After 10 s waiting time, the M versus T curve is measured in a heating cycle after sudden removal of field. Being a zero-field measurement, TRM is likely to be advantageous in comparison with the traditional in-field χ_{dc} versus T measurements in identification of the GP singularity as the PM contribution to the magnetization is likely to be suppressed. Around T_{irr} , the TRM exhibits a sharp upturn, while a sharp and sudden downturn in M_{TRM}^{-1} versus T curves [insets of Fig. 8] indicate the formation of rare regions at $T_C < T < T^*$.

To find the presence of magnetically ordered rare regions, isothermal remanent magnetization (IRM) at $T_C < T < T^*$ is carried out. In the PM regime, IRM generally falls exponentially with time, while in the GP regime, IRM falls nonexponentially with time because magnetically ordered rare regions would take larger time to reverse its effective spin [2,3]. Long ago, it was proposed that in the GP regime, the spin auto-correlation function $C(t)$ has to be in the form of $C(t) \sim \exp[-A*\ln(t)^{d/(d-1)}]$ for an Ising system and $C(t) \sim \exp[-Bt^{1/2}]$ for a Heisenberg system [2,3]. Figure 9 shows the normalized IRM as a function of time for the two representative samples $x = 0.0$ (150 K), 0.2 (130 K). For the IRM measurement, the samples were cooled from 300 K to desired temperature in the presence of field 1 kOe. After stabilizing the temperature and waiting time up to 100 s, variation of magnetization as a function of time (M versus Time) was measured after immediate removal of the field. Interestingly, IRM data indicate the best fit with the Ising spin model decay scheme (Fig. 9). It shows the lack of agreement with the Heisenberg-like interactions as well as an exponential decay model scheme [$M(t) = M(0) + A*\exp(-\frac{t}{\tau})$] as shown in the inset of Fig. 9. It suggests that instead of the PM state above

T_C , the system is in a magnetically ordered rare region (which slows down the dynamics of spins). The observation of an *Ising-like* interaction is consistent with prior reports, where the nature of spin correlation in the pyrochlore iridates was inferred to be Ising-like [49].

One of the standard methods to characterize the GP behavior is to verify the $\frac{1}{\chi}$ versus T defined by $\chi^{-1} = (T - T_C^{rand})^{1-\lambda}$, where the exponent λ is positive but less than unity. Here T_C^{rand} is the critical temperature of random FM clusters lying above T_C but below T^* . The exact estimation of T_C^{rand} is a serious issue. An appropriate choice should be $T_C^{rand} = \theta_{CW}$ so that efficiently it gives rise to $\lambda \sim 0$ in the PM region [7,12,13]. The value of θ_{CW} is much lower than T_C . So, we approximately choose $T_C^{rand} = T_C$. Figure 10(a) shows $\log_{10}(\chi^{-1})$ versus $\log_{10}(\frac{T-T_C^{rand}}{T_C^{rand}})$ plots. Fitting of the linear regime according to the GP equation gives nonzero values of λ ranging between $0 \leq \lambda \leq 1$. The value of λ decreases systematically against Cr doping concentration [Fig. 10(b)]. We further estimate the value of normalized range of $GP_{Norm} = (\frac{T^*-T_C}{T_C})$ [7,11] are given in Table I. The estimated value

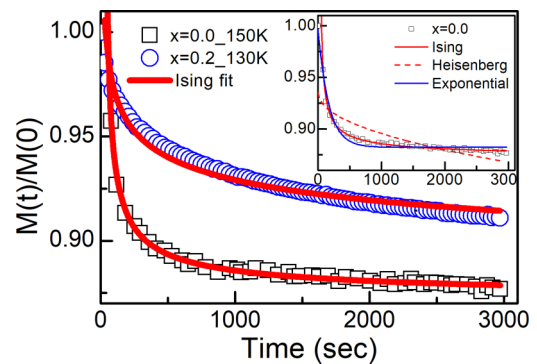


FIG. 9. Variation of normalized IRM with time decay measured at $T_C < T < T^*$ for the $x = 0.0$ (150 K) and $x = 0.2$ (130 K) samples, fitted with Ising model. Inset shows fitting at 150 K of $x = 0.0$ sample along with their Ising, Heisenberg, and exponential model.

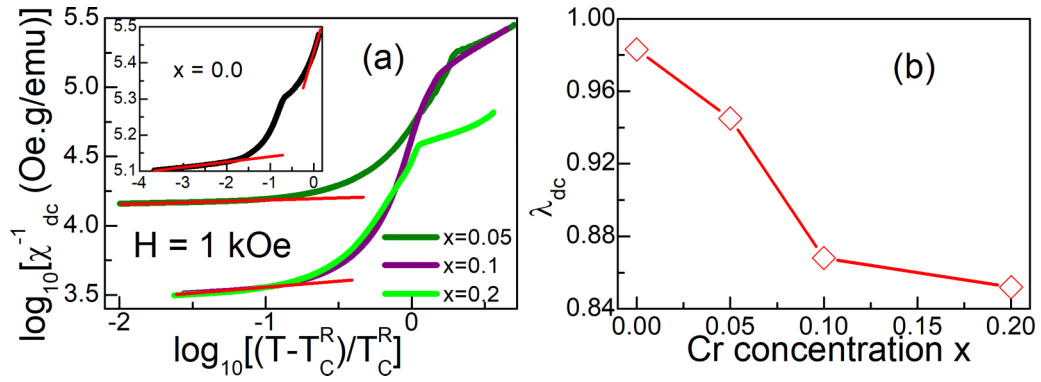


FIG. 10. (a) The temperature-dependent susceptibility data, plotted in log-log scale. For clarity, $x = 0.0$ sample is shown in inset. (b) Dependence of the GP parameters with doping.

of GP_{norm} is greater in the substituted sample (one order) as compared to the $x = 0.0$ sample. Moreover, the YICO series shows significant enhancement in the value of GP_{norm} compared to other systems [9–11,13].

Further, we look into the possible macroscopic origin of the formation of magnetically ordered rare regions. In the parent compound, the Ir site creates local disorder in the pyrochlore crystal structure with the doping of the Cr ion as reported by Refs. [26,27]. As the undoped compound is a disordered system exhibiting strong distorted cubic structure, the quenched disorder (a prerequisite of the GP) is inherent in the system. There are several reports on GP which emerged due to B -site [7,15,50] disorder with mixed oxidation states of transition metal ions. Distortion leads to the coexistence of mixed valence states of Ir, i.e., Ir^{4+} and Ir^{5+} in YICO series. Now, the random distribution of vacancies at the Ir^{4+} site locally reduces the $Ir^{4+} - Ir^{4+}$ interionic bond length where short-range correlations are prevalent. It leads to the coexistence of two phases within the same crystalline state, consistent with other systems exhibiting geometrically frustrated AFM spin arrangement [11–13].

IV. CONCLUSIONS

We investigate the experimental evidence of GP-like behavior in Cr-doped geometrically frustrated AFM pyrochlore iridates $Y_2Ir_2O_7$. In a nutshell, the important observations are as follows: (1) hysteresis in M versus H curve, cusp in χ_{ZFC}

versus T data at lower temperature than irreversible temperature T_{irr} , and relaxation in M versus time curve, suggesting a cluster-glass-like state in the YICO series; (2) a larger value of $\mu_{\text{eff}}^{\text{exp}}$ than $\mu_{\text{eff}}^{\text{theo}}$, suggesting the formation GP-like FM clusters; (3) sudden and sharp downward deviation in $\frac{1}{\chi}$ versus T curves from conventional CW behavior below T^* , a temperature much above the LRO temperature T_C , indicating the formation of magnetically ordered clusters, (4) the $\frac{1}{\chi}$ versus T curves measured at all applied magnetic field do not coincide to a single curve above T^* in the true PM regime; and (6) slow dynamics of spin in IRM data at $T_C < T < T^*$, exhibiting Ising-like interaction, favors the presence of magnetically ordered rare regions. Eventually, all experimental observations suggest the presence of magnetically ordered rare regions in the global PM matrix range $T_C < T < T^*$, favoring GP-like state in YIO. The strength of magnetically ordered rare regions enhances with the substitution of Cr. Rare regions are distributed over a wide temperature regime. It is the maiden study of the GP along with cluster-glass-like states in the geometrically frustrated AFM pyrochlore oxide family. The current finding is important and justifies its importance among the rare materials which exhibit GP along with glass-like states in AFM ordered systems, which is very limited to date.

ACKNOWLEDGMENT

V.K.D. thanks Professor Soumik Mukhopadhyay (IIT Kanpur) for his guidance during this project.

-
- [1] K. Binder and A. P. Young, Spin glasses: Experimental facts, theoretical concepts, and open questions, *Rev. Mod. Phys.* **58**, 801 (1986).
- [2] M. Randeria, J. P. Sethna, and R. G. Palmer, Low-Frequency Relaxation in Ising Spin-Glasses, *Phys. Rev. Lett.* **54**, 1321 (1985).
- [3] A. J. Bray, Nature of the Griffiths Phase, *Phys. Rev. Lett.* **59**, 586 (1987).
- [4] R. B. Griffiths, Nonanalytic Behavior Above the Critical Point in a Random Ising Ferromagnet, *Phys. Rev. Lett.* **23**, 17 (1969).
- [5] J. Deisenhofer, D. Braak, H.-A. K. v. Nidda, J. Hemberger, R. M. Eremina, V. A. Ivanshin, A. M. Balbashov, G. Jug, A. Loidl, T. Kimura, and Y. Tokura, Observation of a Griffiths Phase in Paramagnetic $La_{1-x}Sr_xMnO_3$, *Phys. Rev. Lett.* **95**, 257202 (2005).
- [6] M. B. Salamon, P. Lin, and S. H. Chun, Colossal Magnetoresistance is a Griffiths Singularity, *Phys. Rev. Lett.* **88**, 197203 (2002).
- [7] A. K. Pramanik and A. Banerjee, Griffiths phase and its evolution with Mn-site disorder in the half-doped manganite $Pr_{0.5}Sr_{0.5}Mn_{1-y}Ga_yO_3$ ($y = 0.0, 0.025, \text{ and } 0.05$), *Phys. Rev. B* **81**, 024431 (2010).
- [8] V. K. Shukla and S. Mukhopadhyay, Antiferromagnetic rare region effect in $Pr_{0.5}Ca_{0.5}MnO_3$, *Phys. Rev. B* **97**, 054421 (2018).

- [9] V. K. Dwivedi, and S. Mukhopadhyay, Suppression of long range magnetic ordering and electrical conduction in $Y_{1.7}Bi_{0.3}Ir_2O_7$ thin film, *J. Magn. Magn. Mater.* **484**, 313 (2019); V. K. Dwivedi, Evolution of structural, magnetic and electrical transport properties of $Y_{1.7}Bi_{0.3}Ir_2O_7$ thin film grown on YSZ(100) substrate by PLD, *Phys. B: Condens. Matter* **571**, 137 (2019).
- [10] C. Magen, P. A. Algarabel, L. Morellon, J. P. Araújo, C. Ritter, M. R. Ibarra, A. M. Pereira, and J. B. Sousa, Observation of a Griffiths-Like Phase in the Magnetocaloric Compound $Tb_5Si_2Ge_2$, *Phys. Rev. Lett.* **96**, 167201 (2006).
- [11] Z. W. Ouyang, N. M. Xia, Y. Y. Wu, S. S. Sheng, J. Chen, Z. C. Xia, L. Li, and G. H. Rao, Short-range ferromagnetic correlations in the spin-chain compound Ca_3CoMnO_6 , *Phys. Rev. B* **84**, 054435 (2011).
- [12] J. Kumar, S. N. Panja, S. Dengre, and S. Nair, Identification of a Griffiths singularity in a geometrically frustrated antiferromagnet, *Phys. Rev. B* **95**, 054401 (2017).
- [13] K. Ghosh, C. Mazumdar, R. Ranganathan, and S. Mukherjee, Griffiths phase behaviour in a frustrated antiferromagnetic intermetallic compound, *Sci. Rep.* **5**, 15801 (2015).
- [14] E. V. Sampathkumaran, N. Mohapatra, S. Rayaprol, and K. K. Iyer, Magnetic anomalies in the spin-chain compound Sr_3CuRhO_6 : Griffiths-phase-like behavior of magnetic susceptibility, *Phys. Rev. B* **75**, 052412 (2007).
- [15] A. Pal, P. Singh, V. K. Gangwar, S. Ghosh, P. Prakash, S. K. Saha, A. Das, M. Kumar, A. K. Ghosh, and S. Chatterjee, B-site disorder driven multiple-magnetic phases: Griffiths phase, re-entrant cluster glass, and exchange bias in Pr_2CoFeO_6 , *Appl. Phys. Lett.* **114**, 252403 (2019).
- [16] W. W.-Krempa, G. Chen, Y. B. Kim, and L. Balents, Correlated quantum phenomena in the strong spin-orbit regime, *Annu. Rev. Condens. Matter Phys.* **5**, 57 (2014).
- [17] X. Wan, A. M. Turner, A. Vishwanath, and S. Y. Savrasov, Topological semimetal and Fermi-arc surface states in the electronic structure of pyrochlore iridates, *Phys. Rev. B* **83**, 205101 (2011).
- [18] A. Juyal, A. Agarwal, and S. Mukhopadhyay, Evidence of density waves in single-crystalline nanowires of pyrochlore iridates, *Phys. Rev. B* **95**, 125436 (2017); A. Juyal, Negative Longitudinal Magnetoresistance in the Density Wave Phase of $Y_2Ir_2O_7$, *Phys. Rev. Lett.* **120**, 096801 (2018).
- [19] N. Aito, M. Soda, Y. Kobayashi and M. Sato, Spin glass-like transition and Hall resistivity of $Y_{2-x}Bi_xIr_2O_7$, *J. Phys. Soc. Jpn.* **72**, 1226 (2003).
- [20] N. Taira, M. Wakeshima, and Y. Hinatsu, Magnetic properties of iridium pyrochlores $R_2Ir_2O_7$ ($R = Y, Sm, Eu$ and Lu), *J. Phys.: Condens. Matter* **13**, 5527 (2001).
- [21] W. K. Zhu, M. Wang, B. Seradjeh, F. Yang, and S. X. Zhang, Enhanced weak ferromagnetism and conductivity in hole-doped pyrochlore iridate $Y_2Ir_2O_7$, *Phys. Rev. B* **90**, 054419 (2014).
- [22] B. Ghosh, V. K. Dwivedi, and S. Mukhopadhyay, Non-Fermi liquid regime in metallic pyrochlore iridates: Quantum Griffiths singularities, *Phys. Rev. B* **102**, 144444 (2020).
- [23] H. Kumar, R. S. Dhaka, and A. K. Pramanik, Evolution of structure, magnetism, and electronic transport in the doped pyrochlore iridate $Y_2Ir_{2-x}Ru_xO_7$, *Phys. Rev. B* **95**, 054415 (2017).
- [24] H. Kumar, and A. K. Pramanik, Nonmagnetic substitution in pyrochlore iridate $Y_2(Ir_{1-x}Ti_x)_2O_7$: Structure, magnetism, and electronic properties, *J. Phys. Chem. C* **123**, 13036 (2019).
- [25] H. Kumar, K. C. Kharkwal, K. Kumar, K. Asokan, A. Banerjee, and A. K. Pramanik, Magnetic and transport properties of the pyrochlore iridates $(Y_{1-x}Pr_x)_2Ir_2O_7$: Role of $f-d$ exchange interaction and $d-p$ orbital hybridization, *Phys. Rev. B* **101**, 064405 (2020).
- [26] V. K. Dwivedi, and S. Mukhopadhyay, Coexistence of high electrical conductivity and weak ferromagnetism in Cr doped $Y_2Ir_2O_7$ pyrochlore iridates, *J. Appl. Phys.* **125**, 223901 (2019).
- [27] V. K. Dwivedi, P. Mandal, and S. Mukhopadhyay, Frustration induced inversion of magnetocaloric effect and metamagnetic transition in substituted pyrochlore iridates, *ACS Appl. Electron. Mater.* **4**, 1611 (2022).
- [28] V. K. Dwivedi, and S. Mukhopadhyay, Influence of electronic structure parameters on the electrical transport and magnetic properties of $Y_{2-x}Bi_xIr_2O_7$ pyrochlore iridates, *J. Appl. Phys.* **126**, 165112 (2019).
- [29] H. Liu, J. Bian, S. Chen, J. Wang, Y. Feng, W. Tong, Y. Xie, B. Fang, Evolution of magnetism and electrical properties in the doped pyrochlore iridate $Y_2Ir_{2-x}Fe_xO_7$, *J. Magn. Magn. Mater.* **498**, 166214 (2020).
- [30] H. Liu, J. Bian, S. Chen, Y. Wang, Y. Feng, W. Tong, Y. Xie, B. Fang, Enhanced ferromagnetism and Mott variable-range hopping behavior in Cu doped pyrochlore iridate $Y_2Ir_2O_7$, *Phys. B: Condens. Matter* **568**, 60 (2019).
- [31] A. Juyal, V. K. Dwivedi, S. Verma, S. Nandi, A. Agarwal, and S. Mukhopadhyay, Possible transition between charge density wave and Weyl semimetal phase in $Y_2Ir_2O_7$, *Phys. Rev. B* **106**, 155149 (2022).
- [32] V. K. Dwivedi, A. Juyal, and S. Mukhopadhyay, Colossal enhancement of electrical conductivity in $Y_2Ir_2O_7$ nanoparticles, *Mater. Res. Express* **3**, 115020 (2016); V. K. Dwivedi, Structural and magnetic studies of nanocrystalline $Y_2Ir_2O_7$, *AIP Conf. Proc.* **1665**, 050160 (2015).
- [33] D. Lebedev, M. Povia, K. Waltar, P. M. Abdala, I. E. Castelli, E. Fabbri, M. V. Blanco, A. Fedorov, C. Coperet, N. Marzari, and T. J. Schmidt, Highly active and stable iridium pyrochlores for oxygen evolution reaction, *Chem. Mater.* **29**, 5182 (2017).
- [34] P.-C. Shih, Jaemin Kim, C.-J. Sun, and H. Yang, Single-phase pyrochlore $Y_2Ir_2O_7$ electrocatalyst on the activity of oxygen evolution reaction, *ACS Appl. Energy Mater.* **1**, 3992 (2018).
- [35] M. A. Hubert, A. Gallo, Y. Liu, E. Valle, J. Sanchez, D. Sokaras, R. Sinclair, L. A. King, and T. F. Jaramillo, Characterization of a dynamic $Y_2Ir_2O_7$ catalyst during the oxygen evolution reaction in acid, *J. Phys. Chem. C* **126**, 1751 (2022).
- [36] X. Liu, F. Wen, E. Karapetrova, J.-W. Kim, P. J. Ryan, J. W. Freeland, M. Terilli, T.-C. Wu, M. Kareev, and J. Chakhalian, *In-situ* fabrication and transport properties of (111) $Y_2Ir_2O_7$ epitaxial thin film, *Appl. Phys. Lett.* **117**, 041903 (2020).
- [37] M. C. Shapiro, S. C. Riggs, M. B. Stone, C. R. d. I. Cruz, S. Chi, A. A. Podlesnyak, and I. R. Fisher, Structure and magnetic properties of the pyrochlore iridate $Y_2Ir_2O_7$, *Phys. Rev. B* **85**, 214434 (2012).
- [38] S. M. Disseler, C. Dhital, A. Amato, S. R. Giblin, C. d. I. Cruz, S. D. Wilson, and M. J. Graf, Magnetic order in the pyrochlore iridates $A_2Ir_2O_7$ ($A = Y, Yb$), *Phys. Rev. B* **86**, 014428 (2012).
- [39] S. M. Disseler, Direct evidence for the all-in/all-out magnetic structure in the pyrochlore iridates from muon spin relaxation, *Phys. Rev. B* **89**, 140413(R) (2014).
- [40] T. M. Fernandez, Magnetic characterization of $Y_{2-x}Bi_xIr_2O_7$: A muon spin rotation/relaxation and susceptibility study, M.Sc.

- thesis, McMaster University, 2014, <http://hdl.handle.net/11375/16485>.
- [41] A. Julia, Muon-spin relaxation study of Ir-spin fluctuations in hole-doped pyrochlore iridates $(Y_{1-x-y}Cu_xCa_y)_2Ir_2O_7$, Ph.D. Thesis, Hokkaido University, 2019, <http://hdl.handle.net/2115/82766>.
- [42] H. Kumar, and A. K. Pramanik, Nonequilibrium low temperature phase in pyrochlore iridate $Y_2Ir_2O_7$: Possibility of glass-like dynamics, *J. Magn. Magn. Mater.* **409**, 20 (2016).
- [43] H. Liu, W. Tong, L. Ling, S. Zhang, R. Zhang, L. Zhang, L. Pi, C. Zhang, Y. Zhang, Magnetic order, spin dynamics and transport properties of the pyrochlore iridate $Y_2Ir_2O_7$, *Solid State Commun.* **179**, 1 (2014).
- [44] V. K. Dwivedi, and S. Mukhopadhyay, Effect of stoichiometry on magnetic and transport properties in polycrystalline $Y_2Ir_2O_7$, *AIP Conf. Proc.* **1953**, 120002 (2018); V. K. Dwivedi, Study of optical properties of polycrystalline $Y_2Ir_2O_7$, *ibid.* **1832**, 090016 (2017).
- [45] Y. M. Liang, Z. J. Wang, Y. Bai, Y. J. Wu, X. K. Ning, X. F. Xiao, X. G. Zhao, W. Liu, and Z. D. Zhang, Interface-induced transition from a cluster glass state to a spin glass state in $LaMnO_3/BiFeO_3$ heterostructures, *J. Mater. Chem. C* **7**, 2376 (2019).
- [46] C. He, M. A. Torija, J. Wu, J. W. Lynn, H. Zheng, J. F. Mitchell, and C. Leighton, Non-Griffiths-like clustered phase above the Curie temperature of the doped perovskite cobaltite $La_{1-x}Sr_xCoO_3$, *Phys. Rev. B* **76**, 014401 (2007).
- [47] M. M. Saber, M. Egilmez, A. I. Mansour, I. Fan, K. H. Chow, and J. Jung, Evolution of Curie-Weiss behavior and cluster formation temperatures in Ru-doped $Sm_{0.55}Sr_{0.45}MnO_3$ manganites, *Phys. Rev. B* **82**, 172401 (2010).
- [48] A. Kumar, and R. S. Dhaka, Unraveling magnetic interactions and the spin state in insulating $Sr_{2-x}La_xCoNbO_6$, *Phys. Rev. B* **101**, 094434 (2020).
- [49] L. Savary, E.-G. Moon, and L. Balents, New Type of Quantum Criticality in the Pyrochlore Iridates, *Phys. Rev. X* **4**, 041027 (2014).
- [50] R. S. Silva, Jr., C. Santos, M. T. Escote, B. F. O. Costa, N. O. Moreno, S. P. A. Paz, R. S. Angélica, and N. S. Ferreira, Griffiths-like phase, large magnetocaloric effect, and unconventional critical behavior in the $NdSrCoFeO_6$ disordered double perovskite, *Phys. Rev. B* **106**, 134439 (2022).